# Crystal Structure of Inhibitor-Bound P450BM-3 Reveals Open Conformation of Substrate Access Channel[†,‡]

Donovan C. Haines,[§] Baozhi Chen,[||] Diana R. Tomchick,[||] Muralidhar Bondlela,[||] Amita Hegde,[||] Mischa Machius,[||] and Julian A. Peterson*[,||]

*Department of Biochemistry, The University of Texas Southwestern Medical Center at Dallas, Dallas, Texas 75390-9038, and Department of Chemistry, The University of Texas at Dallas, Dallas, Texas 75083-0688*

*Received December 7, 2007; Revised Manuscript Received January 28, 2008*

ABSTRACT: P450BM-3 is an extensively studied P450 cytochrome that is naturally fused to a cytochrome P450 reductase domain. Crystal structures of the heme domain of this enzyme have previously generated many insights into features of P450 structure, substrate binding specificity, and conformational changes that occur on substrate binding. Although many P450s are inhibited by imidazole, this compound does not effectively inhibit P450BM-3. ω-Imidazolyl fatty acids have previously been found to be weak inhibitors of the enzyme and show some unusual cooperativity with the substrate lauric acid. We set out to improve the properties of these inhibitors by attaching the ω-imidazolyl fatty acid to the nitrogen of an amino acid group, a tactic that we used previously to increase the potency of substrates. The resulting inhibitors were significantly more potent than their parent compounds lacking the amino acid group. A crystal structure of one of the new inhibitors bound to the heme domain of P450BM-3 reveals that the mode of interaction of the amino acid group with the enzyme is different from that previously observed for acyl amino acid substrates. Further, required movements of residues in the active site to accommodate the imidazole group provide an explanation for the low affinity of imidazole itself. Finally, the previously observed cooperativity with lauric acid is explained by a surprisingly open substrate-access channel lined with hydrophobic residues that could potentially accommodate lauric acid in addition to the inhibitor itself.

P450BM-3[1] is a cytochrome P450 from *Bacillus megaterium* that is capable of fatty acid hydroxylation and epoxidation (*1–3*). This enzyme has long served as a model for human P450s and as a uniquely self-sufficient example of a cytochrome P450 naturally fused to a P450 reductase (*4, 5*). The enzyme has a P450 domain, an FMN-binding domain, and an FAD-binding domain, allowing it to receive electrons directly from NADPH in support of extremely fast (>3000 $min^{-1}$) fatty acid oxidation utilizing molecular oxygen to produce oxygenated product and water (*6, 7*). These unique features have made it an attractive system for studying P450 structure and function (*8–12*), as a protein engineering template for biotechnological applications (*13–20*), and as a target template for generating artificial P450−P450 reductase fusions of human P450s (*21–23*).

Many P450s are inhibited by imidazole, as the $sp^2$-hybridized nitrogen of imidazole is a very good ligand for the heme iron. Bound imidazole blocks access of oxygen to P450s required for turnover (*24–26*). Imidazole is not a good inhibitor of P450BM-3, presumably due to nonproductive steric interactions in the active site of this enzyme. Inhibitors that incorporate an imidazole moiety in a fatty acyl chain to enhance affinity for the enzyme have been developed, but the affinity for P450BM-3 is relatively weak (5–200 μM $K_D$). Additionally, the binding kinetics for some of these analogues are complex and not well understood (*26*). These results suggest the presence of a somewhat rigid, constrained active site in the immediate vicinity of the heme iron in P450BM-3. By contrast, analysis of many substrate-free and substrate-bound structures of the enzyme, along with recent molecular dynamics calculations (*27, 28*), suggests that there is significant flexibility in the active site.

Recently we have shown that N-fatty acylated amino acids are much better substrates for P450BM-3 than the corresponding fatty acids, due to increased affinity for the enzyme and improved water solubility (*11, 29*). In order to further probe the active site plasticity of P450BM-3, we have generated *N*-(ω-imidazolyl fatty acyl)-L-amino acid inhibitors. The inhibitors had a much higher affinity for the enzyme, and determination of the crystal structure of one of them in complex with the heme domain of P450BM-3 reveals new insight into the plasticity of active site residues in the immediate vicinity of the heme iron. The structure also provides an explanation for the unusual cooperativity previously observed for the ω-imidazolyl fatty acid-based inhibitors.

[†] This research was supported in part by Research Grants GM43479 and GM50858 from the NIH. Results shown in this report are derived from work performed at Argonne National Laboratory, Structural Biology Center at the Advanced Photon Source. Argonne is operated by UChicago, Argonne, LLC, for the U.S. Department of Energy, Office of Biological and Environmental Research under Contract DE-AC02-06CH11357.

[‡] Coordinates and structure factors have been deposited in the Protein Data Bank under Accession Number 3BEN.

* Corresponding author. E-mail: Julian.Peterson@UTSouthwestern.edu. Phone: 214-648-2361. Fax: 214-645-9361.

[§] The University of Texas at Dallas.

[||] The University of Texas Southwestern Medical Center at Dallas.

10.1021/bi7023964 CCC: $40.75 
Published on Web 02/26/2008

## EXPERIMENTAL PROCEDURES

*General Methods.* The heme-binding domain of P450BM-3 and the holoenzyme were purified as previously described (*30, 31*). The concentrations of BMP and P450BM-3 were determined by the method of Omura and Sato (*32*). UV–visible spectroscopy was performed on either a Hewlett-Packard model 8452A diode array spectrophotometer or a Varian Cary model 100 double beam spectrophotometer. Acyl amino acid substrates were prepared as described (*29*).

*10-Imidazolyldecanoic Acid and 12-Imidazolyldodecanoic Acid.* ω-Imidazolyl fatty acid methyl esters were prepared from the corresponding ω-bromo fatty acid esters and subsequently hydrolyzed by previously published methods (*33, 34*). Purity and identity were confirmed by $^1$H NMR and GC-MS.

*N-(10-Imidazolyldecanoyl)glycine.* 10-Imidazolyldecanoic acid methyl ester was coupled to glycine by a procedure previously used to couple similar compounds to peptide antifungals (*35*). 10-Imidazolyldecanoic acid methyl ester (0.15 g, 0.63 mmol), 1-[3-(dimethylamino)propyl]-3-ethylcarbodiimide (0.12 g, 0.63 mmol), and 1-hydroxybenzotriazole (0.085 g, 0.63 mmol) were added to 8 mL of anhydrous DMF, stirred for 1.5 h at room temperature, and then cooled to 0 °C. Glycine methyl ester hydrochloride (0.078 g, 0.63 mmol) was dissolved in 4 mL of anhydrous DMF with triethylamine (0.063 mg, 0.63 mmol), and this mixture was added to the stirring reaction at 0 °C over 15 min. The reaction was then allowed to warm to room temperature and stirred for an additional 15 h. The solvent was removed under vacuum. The reaction mixture was taken up in 10 mL of $CH_2Cl_2$, washed with saturated $NaHCO_3$ three times and brine three times, and dried over $Na_2SO_4$. The crude product was purified by preparative TLC on silica using 10% MeOH/$CH_2Cl_2$ to obtain 0.123 g (64%). Essentially quantitative ester hydrolysis of the methyl ester (50 mg, 0.16 mmol) was accomplished in 3 mL of 2:1 THF:$H_2O$ and adding 13.6 mg (0.32 mmol) of LiOH/$H_2O$ at room temperature. The mixture was stirred for 10 h at room temperature. The THF was evaporated under reduced pressure, the aqueous remnant was acidified to pH 6 with HCl at 0 °C, and the solid precipitate was collected by filtration. The final purified yield was 64%. $^1$H NMR (400 MHz, $CD_3OD$): δ 1.34 (s, 10H), 1.63 (m, 2H), 1.84 (m, 2H), 2.26 (t, 2H), 3.84 (s, 2H), 4.11 (t, 2H), 7.17 (s, 1H), 7.31 (s, 1H), 8.1 (s, 1H).

*N-(12-Imidazolyldodecanoyl)glycine.* This compound was made in a manner identical to *N*-(10-imidazolyldecanoyl)glycine with the exception that 10-imidazolyldecanoic acid methyl ester was replaced by 12-imidazolyldodecanoic acid methyl ester. $^1$H NMR (400 MHz, $CD_3OD$): δ 1.34 (s, 14H), 1.63 (m, 2H), 1.84 (m, 2H), 2.26 (t, 2H), 3.84 (s, 2H), 4.11 (t, 2H), 7.17 (s, 1H), 7.31 (s, 1H), 8.1 (s, 1H).

*N-(10-Imidazolyldecanoyl)-L-leucine.* This compound was made in a manner identical to *N*-(10-imidazolyldecanoyl)glycine with the exception that the glycine methyl ester hydrochloride was replaced by leucine methyl ester hydrochloride. $^1$H NMR (400 MHz, $CD_3OD$): δ 0.95 (dd, 6H), 1.31 (s, 10H), 1.56–1.75 (m, 5H), 1.84 (m, 2H), 2.24 (t, 2H), 4.08 (t, 2H), 4.42 (dd, 1H) 7.12 (s, 1H), 7.26 (s, 1H), 7.96 (s, 1H).

*N-(12-Imidazolyldodecanoyl)-L-leucine.* This compound was made in a manner identical to *N*-(12-imidazolyldecanoyl)glycine with the exception that the glycine methyl ester hydrochloride was replaced by leucine methyl ester hydrochloride. $^1$H NMR (400 MHz, $CD_3OD$): δ 0.95 (dd, 6H), 1.31 (s, 14H), 1.56–1.75 (m, 5H), 1.84 (m, 2H), 2.24 (t, 2H), 4.08 (t, 2H), 4.42 (dd, 1H) 7.12 (s, 1H), 7.26 (s, 1H), 7.96 (s, 1H).

*Inhibitor Characterization.* For spectrophotometric titrations, 1.2 mL of a solution of 2.5 μM BMP in 50 mM potassium phosphate buffer (pH 7.4) was titrated with a solution of 1 mM inhibitor in 50 mM potassium carbonate in a stirred 1.00 cm quartz cuvette. After addition of each aliquot of substrate, the solution was allowed to equilibrate for 1 min before the UV–visible absorbance spectrum was recorded. For increased sensitivity, absorbance at 422 nm was subtracted from the absorbance at 418 nm, and the data were fitted to a dilution-correcting equation for a bimolecular association reaction to obtain dissociation constants (*11*).

For the measurement of NADPH consumption, a solution of 100 μM laurate and 100 μM NADPH in 50 mM potassium phosphate buffer (pH 7.4) was placed in a 1.00 mL cuvette at 25 °C. Inhibitor, where included, was present at a concentration of 100 μM, and the reaction was initiated by the addition of P450BM-3 to a final concentration of 50 nM. The loss of UV–visible absorption at 340 nm, indicating NADPH consumption, was monitored. For the calculation of NADPH concentrations an extinction coefficient of 6220 $M^{-1}$ $cm^{-1}$ at 340 nm for NADPH was used.

*Complex Formation and Crystallization.* For complex formation, BMP (20 μM BMP in 50 mM potassium phosphate, pH 7.4) was titrated with 10 mM *N*-(12-imidazolyldodecanoyl)-L-leucine in 50 mM potassium carbonate to 10% beyond the equivalence point. The extent of complex formation was established by monitoring the changes in the UV–visible spectrum. This solution was then concentrated in an Amicon Centriprep-30 concentrator to a final concentration of 105 μM (12.5 mg/mL). The solution was stored in small aliquots at −80 °C.

Crystals of the BMP/*N*-(12-imidazolyldodecanoyl)-L-leucine complex (BMP/C12-Im-Leu) were grown using the vapor diffusion method in the sitting drop format using methods similar to those previously described for the BMP/*N*-palmitoyl-L-methionine crystal structure (*29*). Precipitant solution was composed of 11% (w/v) PEG-3350, 200 mM magnesium chloride, 7.5% (v/v) glycerol, and 100 mM MES, pH 6.0. Equal volumes (2 μL each) of the 4 °C well solution and the 12.5 mg/mL BMP/C12-Im-Leu complex were mixed by pipet, and the wells were sealed. After equilibration for 24 h at 4 °C, crystallization was induced by streak seeding from lower quality crystals grown spontaneously at higher PEG-3350 concentrations. Large numbers of crystals typically formed within 24 h. Crystals were transferred to a solution composed of 13% (w/v) PEG-3350, 7.5% (v/v) glycerol, 200 mM magnesium chloride, 100 mM MES, pH 6.0, supplemented with 20% (v/v) ethylene glycol and incubated 1 h for cryoprotection before being mounted in a nylon loop. To minimize damage to the crystals, cryoprotectant was added to the crystallization drop and a compensating volume subsequently removed in multiple steps until the final solution composition was reached. Mounted crystals were flash-cooled in liquid propane and stored in liquid nitrogen until used for X-ray diffraction data collection.

*Data Collection, Structure Determination, and Refinement.* Diffraction data from a single crystal were collected at 100 K at beamline 19-BM of the Argonne National Laboratory Structural Biology Center at the Advanced Photon Source. Data sets were indexed, integrated, and scaled using the HKL2000 program package (*36*). BMP/*N*-(12-imidazolyldodecanoyl)-L-leucine crystals exhibited the symmetry of space group $P2_1$ with unit cell parameters $a = 58.8$ Å, $b = 148.2$ Å, $c = 63.8$ Å, $\beta = 98.3$ °, diffracted X-rays to a minimum Bragg spacing ($d_{min}$) of 1.65 Å, and contained two molecules in the asymmetric unit (50% solvent). The structure was determined by the difference Fourier method. The initial model consisted of the coordinates of BMP in complex with *N*-palmitoylglycine [PDB code: 1JPZ (*11*)] with the coordinates for the substrate and water molecules removed. Rigid-body refinement of the model coordinates versus data between 30.0 and 1.65 Å was conducted. As the conformation of the BMP was intermediate between the fully closed form of *N*-palmitoylglycine-bound BMP and the open, substrate-free form, extensive manual model rebuilding in the program O (*37*) was followed by cycles of simulated annealing refinement in the program CNS (version 1.1) (*38*). Subsequent cycles of refinement in CNS included standard positional and isotropic atomic displacement parameter refinement and addition of water molecules where chemically reasonable. In the final stages of refinement, inspection of electron density maps allowed a model for the substrate to be added. Final model refinement was performed in REFMAC (version 5.2) *(39)* and included TLS refinement. The model that was fit to data obtained from *N*-(12-imidazolyldodecanoyl)-L-leucine-bound BMP crystals included one heme group per monomer in two alternate conformations, one *N*-(12-imidazolyldodecanoyl)-L-leucine per monomer, one molecule of MES, one $Mg^{2+}$, 904 water molecules, and all protein residues except A1−A3, A458−A470, and B458−B470. Data collection and refinement statistics are detailed in Table 1.

*Structure Figures.* All figures of *N*-(12-imidazolyldodecanoyl)-L-leucine-bound BMP structures were constructed using the PyMOL or MacPyMOL programs (*40*).

Table 1: Data Collection and Refinement[a]

| | |
|---|---|
| **Data Collection** | |
| wavelength (Å) | 0.97959 |
| resolution range (Å) | 35.2−1.65 (1.68–1.65) |
| unique reflections | 125826 (5307) |
| multiplicity | 4.3 (3.7) |
| data completeness (%) | 97.2 (81.7) |
| $R_{merge}$ (%)[b] | 4.8 (24.9) |
| $I/\sigma(I)$ | 26.1 (4.4) |
| Wilson *B*-value (Å$^2$) | 17.6 |
| **Refinement Statistics** | |
| resolution range (Å) | 29.60−1.65 (1.69–1.65) |
| no. of reflections $R_{work}/R_{free}$ | 121940/3825 (7694/245) |
| atoms (non-H protein/heme/ solvent/inhibitor) | 7544/172/917/54 |
| $R_{work}$ (%) | 16.1 (16.8) |
| $R_{free}$ (%) | 19.1 (21.5) |
| rmsd bond length (Å) | 0.015 |
| rmsd bond angle (deg) | 1.70 |
| mean *B*-value (protein/heme/ solvent/inhibitor) (Å$^2$) | 23.7/11.5/34.4/44.2 |
| $\sigma_A$ coordinate error (Å) | 0.053 |
| alternate conformations | 26 residues, 2 hemes |
| Ramachandran outliers | A, His266; B, His266 |
| missing residues | A, 1–3, 458–470; B, 458–470 |

[a] Data for the outermost shell are given in parentheses. [b] $R_{merge} = 100\sum_h\sum_i|I_{h,i} - \langle I_h\rangle|/\sum_h\sum_i I_{h,i}$, where the outer sum ($h$) is over the unique reflections and the inner sum ($i$) is over the set of independent observations of each unique reflection.

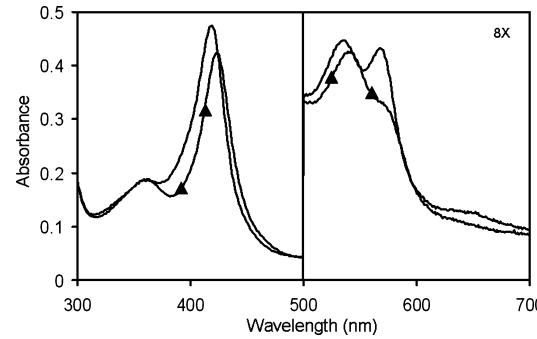


FIGURE 1: Spectroscopic changes upon binding of C12-Im-Leu to BMP. The UV–visible spectrum of 4 $\mu$M BMP (line only) or BMP complexed with C12-Im-Leu (triangles) in 50 mM potassium phosphate, pH 7.4, was recorded.

## RESULTS

*Synthesis and Binding of Imidazole Inhibitors to BMP.* Nitrogen bases have been known for many years to function as inhibitors of some P450s by binding to the heme iron at the same position as the replaceable sixth ligand, a water molecule. Initially, this ligand exchange was observed by difference spectroscopy in microsomal suspensions and was referred to as a "type II" spectral change (*24*). With soluble preparations of P450s such as P450cam, the ligand exchange reaction is observed by a shift in the Soret band of the ferric form of P450s from 418 to 422 nm (*25*). Inhibitors of P450BM-3 incorporating imidazole as a heme ligand have been designed and characterized (*26*). Although the nitrogen base of the imidazole group can be shown to bind to the heme iron by optical absorbance spectroscopy, the equilibrium dissociation constants are only marginally better than that of the parent fatty acid (*26*).

We previously established that fatty acid binding is greatly enhanced by derivatization of the fatty acid carboxylate with amino acids, especially those with hydrophobic side chains (*29*). In this study we set out to utilize the same enhancement to increase the potency of imidazole-based fatty acid inhibitors. These molecules were synthesized as described in Materials and Methods, and their purity was demonstrated by chromatographic and NMR techniques. As can be seen in Figure 1, the addition of the imidazole-based inhibitor to substrate-free BMP resulted in the expected shift of the Soret absorbance band from 418 to 422 nm. Also seen in this figure are the expected absorbance changes that occur in the 500–700 nm portion of the spectrum. Spectrophotometric titrations were performed to determine the dissociation constant for these compounds, and the results are shown in Table 2. The parent compound without the amino acid amide binds rather poorly as shown by the C12-Im derivative, which has a comparable distance from the carboxyl group to the imidazole nitrogen as a C14 or C16 fatty acid (myristic acid or palmitic acid). The addition of amino acid headgroups to the inhibitors was very effective at increasing inhibitor potency. For the C10- and C12-Im derivatives, addition of a glycine headgroup increased affinity 11-fold and 4-fold,

Table 2: Inhibitor Binding to BMP[a]

| compound | $K_D$ ($\mu$M) | compound | $K_D$ ($\mu$M) |
|---|---|---|---|
| palmitic acid | $1.3 \pm 0.2$ | C12-Im-Gly | $1.2 \pm 0.1$ |
| C10-Im | $210 \pm 7$ | *N*-palmitoylleucine | <0.03 |
| C12-Im | $5.2 \pm 0.5$ | C10-Im-Leu | $6.4 \pm 0.9$ |
| *N*-palmitoylglycine | $0.32 \pm 0.01$ | C12-Im-Leu | $0.32 \pm 0.03$ |
| C10-Im-Gly | $18.6 \pm 2.2$ | | |

[a] Dissociation constants were determined using 4.0 $\mu$M BMP in 50 mM potassium phosphate buffer, pH 7.4, titrated with a solution of 1 mM inhibitor in 50 mM potassium carbonate in a stirred 1.00 cm quartz cuvette. The data for the absorbance at 418 nm minus the absorbance at 422 nm were fitted to an equation for the bimolecular association reaction to obtain the dissociation constant.

respectively. Addition of an L-leucine headgroup increased affinity 33-fold and 16-fold, respectively, compared to the fatty acid derivatives. Similar increases in affinity were previously observed for modification of saturated fatty acids with glycine and leucine. For example, the affinity of palmitic acid for P450BM-3 increased 4-fold upon derivatization with glycine and more than 43-fold when derivatized with leucine. In all cases leucine increases affinity more than glycine, although the effect was not quite as pronounced with the inhibitors as with fatty acid substrates.

It should be noted that the binding constant for C12-Im compares well with previous work by Noble et al. (*26*) (5.2 $\mu$M here versus 8.0 $\mu$M in their study), but the binding constants for C10-Im are significantly different (210 $\mu$M here versus $\leq$0.2 $\mu$M in the previous study). Our values are reasonable in light of the known chain length specificity of the enzyme: binding affinity decreases as fatty acyl chain lengths decrease from 15 or 16 carbons (*41*). Further, we consistently see the weaker binding of C10 compounds versus C12 compounds in all three types of compounds (fatty acid and acylglycine- and acylleucine-based inhibitors). Thus, we have a high degree of confidence in that C10-Im compounds bind more weakly than C12-Im in spite of the previous report (*26*).

*Inhibition of Fatty Acid Oxidation by Imidazole Inhibitors.* Although the amino acid derivatives of the imidazole fatty acids bind to oxidized BMP as determined by the change in the absorbance spectrum, we wanted to make sure that these compounds could compete with fatty acids for the substrate binding site. The addition of an equimolar concentration of palmitic acid to BMP results in a conversion of about 30% of the heme iron to the high-spin form. The subsequent addition of an excess of C12-Im-Leu to the reaction mixture resulted in essentially complete conversion of the heme iron from the mixture of low- and high-spin observed in the presence of palmitic acid to the imidazole-bound low-spin form (data not shown). This result indicates that the imidazole derivative binds to BMP even though the fatty acid, palmitic acid in this case, was present in the reaction mixture.

In studies on P450cam, when the inhibitor metyrapone is bound, a Soret absorbance band appears at about 424 nm (*25*). When the heme iron is then reduced from the ferric to the ferrous state, the Soret absorbance band shifts to 448 nm, indicating that this strong-field ligand is still bound to the reduced heme iron. We decided to reduce BMP by adding sodium dithionite to C12-Im-Leu-bound BMP. Interestingly, the absorbance of the Soret band did not shift to longer wavelengths, thus indicating that the imidazole group was no longer a ligand of the heme iron. Also, introducing carbon monoxide into this solution resulted in the appearance of the 446 nm absorbance band of the CO complex, confirming the absence of the imidazole nitrogen−iron bond. This finding is consistent with previous observations (*26*) where no spectral shift could be observed after adding imidazolyl carboxylic acids (C10-Im and C12-Im) to reduced, anaerobic enzyme, leading to the conclusion that the compounds did not bind to reduced enzyme.

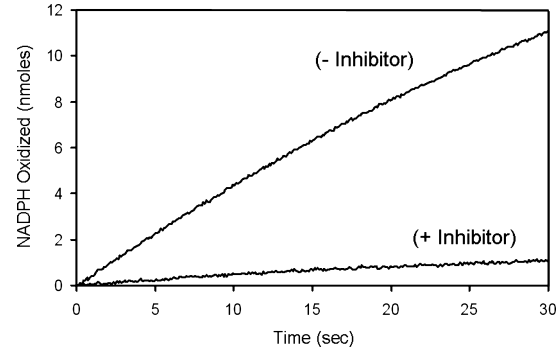


FIGURE 2: Effect of C12-Im-Leu on NADPH-dependent lauric acid oxidation by P450BM-3. NADPH consumption by 50 nM P450BM-3 in a solution of 100 $\mu$M laurate and 100 $\mu$M NADPH in 50 mM potassium phosphate buffer (pH 7.4) was monitored by the loss of absorbance at 340 nm in the UV–visible spectrum. Inclusion of 100 $\mu$M C12-Im-Leu caused a drastic decrease in the rate of NADPH consumption.

Because the imidazole derivatives described in this report form an iron−ligand bond in the ferric form of BMP but not the ferrous form, we decided to examine the ability of this compound to inhibit NADPH oxidation and hydroxylation of lauric acid. Under these conditions, the rate of oxidation of NADPH is inhibited by more than 90%, demonstrating that this compound is a very potent inhibitor of the oxidation of lauric acid (Figure 2).

*Crystal Structure of the BMP/N-(12-Imidazolyldodecanoyl)-L-leucine Complex.* In order to confirm that the increase in affinity was due to the same interactions of the amino acid headgroup of the ligand with the enzyme as were seen for acyl amino acid substrates, a solution of the C12-Im-Leu inhibitor complexed to BMP was prepared and crystallized using conditions similar to those used for *N*-palmitoylglycine/BMP and *N*-palmitoyl-L-methionine/BMP complexes. The crystal structure was then determined by the difference Fourier method using the coordinates for the *N*-palmitoylglycine/BMP structure as the initial model and refined using data to a resolution of 1.65 Å. Statistics for refinement of the BMP structure with bound C12-Im-Leu inhibitor appear in Table 1.

The substrate-free structure of BMP (PDB code 2HPD) has been shown to be more open than the substrate-bound form (*9, 11, 12*). Overall, the backbone of the inhibitor-bound structure determined here resembles substrate-free forms of BMP more than substrate-bound forms (Figure 3). This

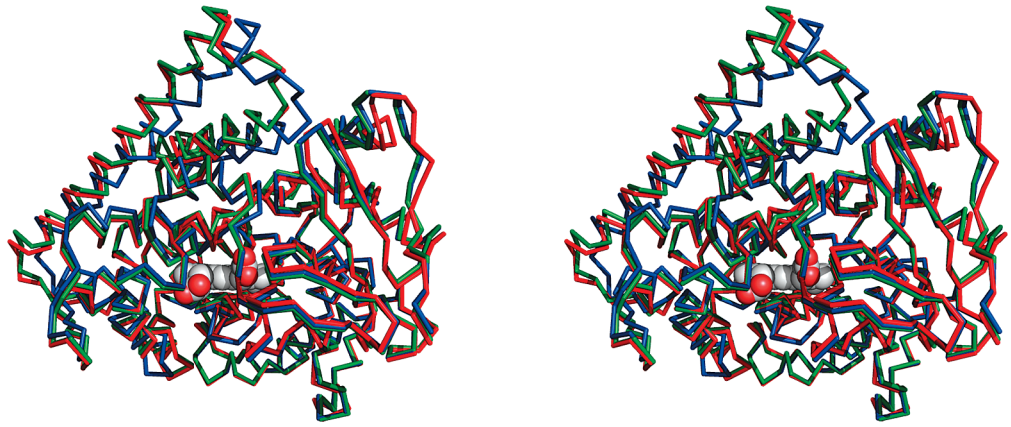

FIGURE 3: Inhibitor-bound BMP resembles substrate-free BMP more than substrate-bound BMP. Backbone trace of the substrate-free (1BU7 monomer B, red), substrate-bound (1JPZ monomer B, blue), and inhibitor-bound (monomer B, green) structures of BMP. The proteins were aligned using the core residues as described previously (*11*). The heme of the substrate-bound structure is shown as filled spheres. The enzymes are oriented with heme propionates pointed toward the reader and the F and G helices, the most variable part of the structures, at top left.

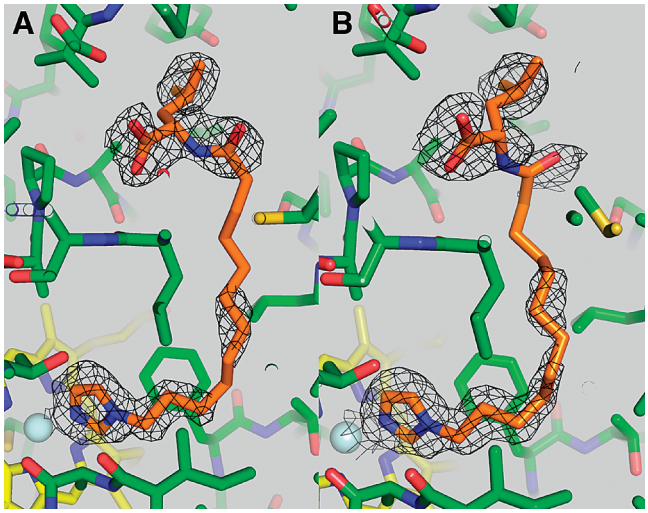


FIGURE 4: Electron density of the bound inhibitor in the enzyme active site. View of the structure of the *N*-(12-imidazolyldodecanoyl)-L-leucine inhibitor in sticks overlaid with a $\sigma_A$-weighted $2F_o - F_c$ electron density omit map contoured at the 0.8$\sigma$ level. The inhibitor is colored orange, the protein is colored green, the heme ring is in yellow and iron is in light cyan. (A) Inhibitor in monomer A. (B) Inhibitor in monomer B.

finding is somewhat surprising, as the inhibitor is very similar in structure to other *N*-acyl amino acids that have been used to characterize the substrate-bound forms. The active site channel exists in a much more open conformation than in substrate-bound BMP structures, which likely contributes to the observed disorder of the inhibitor acyl chains.

The electron density for the inhibitor is well defined in places, but not for the entire compound in both monomers in the asymmetric unit (Figure 4). In both molecules, the imidazole ring and the following three carbons of the acyl chain attached to this ring are well defined, although more of the acyl chain is defined in molecule B than in molecule A. The distance between the coordinating nitrogen of the imidazole ring and the heme iron is about 2.4 Å in each monomer. Although in other structures of P450s complexed to inhibitors with imidazole or pyridine rings the rings of the nitrogen ligands are approximately perpendicular to the I-helix (*42–46*), in the BMP/C12-Im-Leu complex the imidazole ring is essentially parallel to the I-helix. The imidazole ring is very well defined in the electron density, so its orientation in the active site is unambiguous.

There are two possible parallel orientations for the inhibitor molecule. One would allow the acyl chain to extend directly out of the substrate-access channel. We did not observe this orientation in the electron density. Rather, the imidazole ring is oriented parallel to the I-helix, with the acyl chain extending initially toward V78. The acyl chain is well defined in this region (Figure 4). The chain must then change direction toward the substrate-access channel, and at this point, the electron density becomes less well defined. In this region there is significant open space in the substrate-access channel (due to the more open conformation of the enzyme relative to substrate-bound forms), which likely allows conformational disorder of the acyl chain. Finally, the position of the amino acid headgroup is more fixed, with density becoming better defined again.

Perhaps the most surprising feature of inhibitor binding to BMP is the architecture of the binding site for the amino acid headgroup. For both *N*-palmitoylglycine and *N*-palmitoyl-L-methionine, the amino acid carboxylate caps the B′-helix of the enzyme. This feature is responsible for a significant portion of the increased affinity of acyl amino acids relative to fatty acids. For amino acids with hydrophobic side chains like methionine, the side chain rests in a hydrophobic pocket near R47, providing further increases in affinity due to favorable desolvation of the pocket and of the amino acid side chain (*29*). In the C12-Im-Leu structure, however, the amino acid carboxylate faces away from the B′-helix and toward the side-chain carboxylate of E435 and the main-chain carbonyl oxygens of T436 and L437. The leucine side chain nestles in a hydrophobic pocket formed by the side chains of L20, P25, V26, L29, Y51, A330, and M354 (Figure 5). Although the inclusion of a leucine moiety resulted in an increase in affinity for both substrate and inhibitor, the interaction of the amino acid portion with the enzyme is significantly different. The contact with the polar hydroxyl group of Y51 is probably partly responsible for the fact that the addition of the leucine headgroup increased the affinity of this inhibitor only 16-fold, compared to the 43-

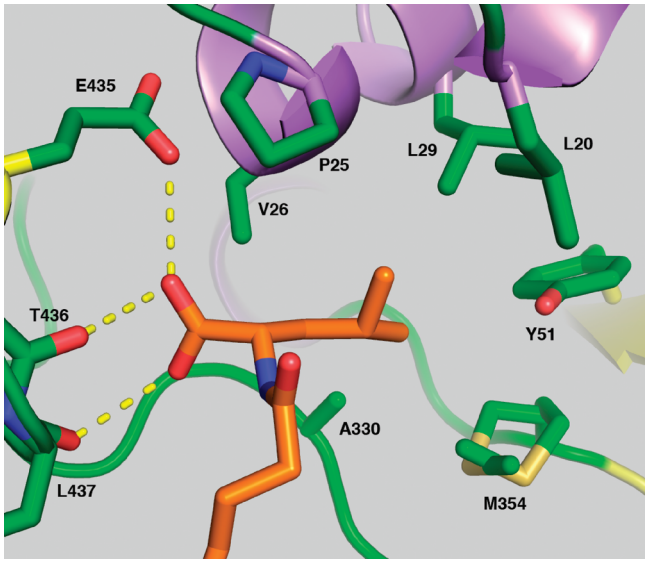


FIGURE 5: Protein residues that line the binding pocket of the leucine amino acid headgroup of the *N*-(12-imidazolyldodecanoyl)-L-leucine inhibitor. The inhibitor is colored orange, protein side chains are colored green, and hydrogen bonds are drawn as dashed yellow lines. Protein helices are in purple, strands are in yellow, and loops are in green. The side chain of M354 was modeled in two conformations.

fold increase in affinity when a leucine headgroup is added to the substrate palmitate.

Significant movements of amino acids in the active site on the distal side of the heme occur to accommodate the new imidazole ligand of the heme iron (Figure 6). The side chain of F87, which has previously been shown to rotate upon substrate binding, has moved away from the heme iron and is in van der Waals contact with the acyl chain of the inhibitor and the nitrogen of the imidazole ring. On the other face of the imidazole ring, the I-helix is significantly distorted. The distortion appears to be due to a steric conflict between the side chain of residue A264 and the imidazole ligand. Due to this steric conflict, neither the substrate-free conformations of A264 and F87 in 1BU7 nor the substrate-bound conformations in 1JPZ can exist simultaneously with the imidazole ring in position as a ligand of the heme iron (Figure 6). The presence of a glycine at position 265 provides backbone conformational flexibility in this region of the P450 I-helix, which allows A264 to move away from the inhibitor imidazole ring, resulting in significant changes in the positions of G265, H266, E267, and the highly conserved threonine, T268. As a result, the backbone torsional angles for H266 change from values consistent with an α-helical geometry ($\varphi$ of about −70°, $\psi$ of approximately −50°) to values falling into the disallowed region of the Ramachandran plot ($\varphi$ of about −85°, $\psi$ of approximately −130°) (*47*). Interestingly, these changes seem to be highly localized to just those residues in the expanded groove of the I-helix, as the backbone on either side of these residues superposes with the equivalent positions in previous substrate-free structures (Figure 7).

## DISCUSSION

Newly discovered interactions accessible in the P450BM-3 active site have allowed the design of novel, extremely potent inhibitors for this enzyme. The expectation was that the increased inhibition was due to the previously discovered interaction of the carboxylates of acyl amino acids with the uncapped N-terminal backbone amides of the B′-helix (*11*). Exploitation of a hydrophobic cleft available to amino acid side chains results in even stronger interactions of the aminoacyl fatty acid analogues with the enzyme.

The new inhibitors incorporating the amino acids glycine or leucine both showed increases in affinity of a magnitude comparable to that observed with similarly derivatized fatty acid substrates. These observations allowed us to increase the affinity of the imidazole inhibitors 20–35-fold by adding a leucine moiety to the ligand. The inhibitors clearly bind to the ferric form of the enzyme, because the spin-state change of the heme iron can be observed to change as the nitrogen ligand replaces the water ligand present in the resting state of the enzyme.

Upon reduction of the enzyme, does the inhibitor dissociate? Spectroscopic experiments indicate that, at a minimum, the imidazole group dissociates from the heme iron. It is not required that the entire inhibitor molecule dissociate from the enzyme active site, however. Upon reduction, the carbon monoxide complex can be formed, so dissociation of the inhibitor must at least make enough room for CO to bind. Because the first electron reduction of P450BM-3 is the rate-limiting step for the enzyme (*48*), it appears, therefore, that the inhibitory effect likely includes a slowing of the initial reduction of the heme iron.

The fact that the inhibitor is released from the enzyme upon heme−iron reduction is interesting for another reason. Since similar inhibitors remain bound to P450cam upon reduction, it was not expected that the Fe−N interaction should break when the enzyme was reduced. Rather, inhibitor release implies that there is a conformational change upon reduction that further restricts access to the heme iron. The existence of a conformational change in the active site of the enzyme when the heme iron is reduced has been suggested before, based on measurements of rates of relaxation of substrate protons in $^1$H NMR (*49, 50*) and analysis of X-ray crystal structures of substrate-bound enzyme (*9, 11*). Consistent with these observations, crystals of *N*-palmitoylglycine in complex with oxidized (resting) BMP were observed to crack and shatter during attempts to anaerobically reduce the complex (*11*). The fact that the imidazole inhibitors are ultimately ejected further supports the existence of a significant conformational change that rearranges the active site in the immediate vicinity of the binding site for the sixth heme iron ligand.

The increase in affinity of the inhibitors for P450BM-3 allowed us to form a more stable complex of the imidazole-containing inhibitors with BMP, leading to a crystal structure of the complex. This structure provides explanations for several prior observations from spectroscopic binding studies and kinetic assays of this class of inhibitor.

First, why does imidazole (and other small aromatic amine based inhibitors) inhibit some P450 enzymes but not CYP102A1? Steric conflict between the imidazole ring and A264 and F87 provides an explanation. The residue that aligns with A264 in some P450s that are inhibited by imidazole is glycine. P450cam, for example, contains a glycine at this position. By contrast, several P450 cytochromes that are inhibited by aromatic amines do have an alanine at this position, including the structurally character-

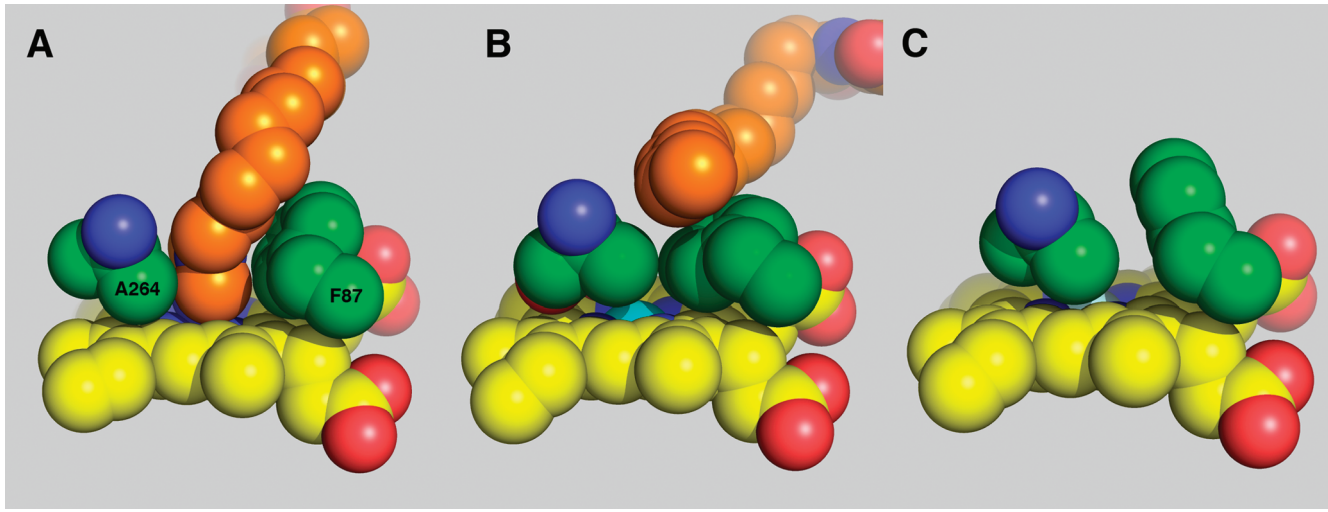


FIGURE 6: Space-filling models of steric constraints and flexibility near the heme iron. (A) Structure of the *N*-(12-imidazolyldodecanoyl)-L-leucine inhibitor (orange) and residues A264 and F87 (green) positioned near the heme (yellow) as they appear in monomer A of the crystal structure. (B) Structure of the *N*-palmitoylglycine substrate (orange) and residues A264 and F87 shown in the conformation of monomer B of substrate-bound BMP (PDB ID code 1JPZ), where they would sterically conflict with the bound *N*-(12-imidazolyldodecanoyl)-L-leucine inhibitor as seen in (A). (C) Residues A264 and F87 shown in the conformation of monomer B of the substrate-free BMP (PDB ID code 1BU7), where they would sterically conflict with the bound *N*-(12-imidazolyldodecanoyl)-L-leucine inhibitor as seen in (A).

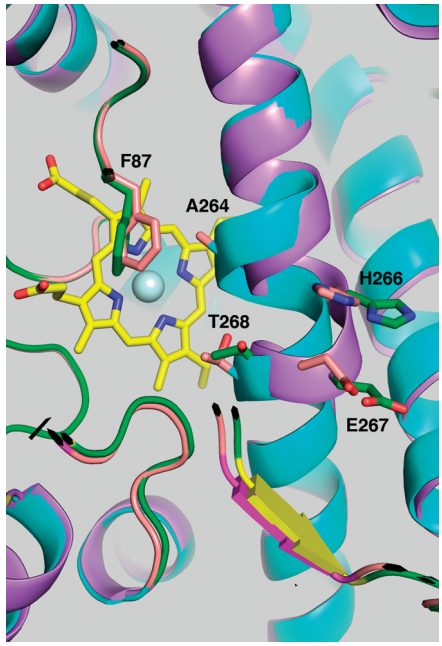


FIGURE 7: The distortion in the I-helix on inhibitor binding. The distortion in the I-helix of the *N*-(12-imidazolyldodecanoyl)-L-leucine inhibitor complex is localized to the expanded groove. A superposition of monomer B of the inhibitor-bound BMP (helices are in violet, strands in yellow, loops and side chains in green) to monomer B of the substrate-free BMP (PDB ID 1BU7) (helices are in cyan, strands in magenta, loops and side chains in tan). The iron atom is shown as a light cyan sphere. For clarity, the inhibitor and the heme from the substrate-free structure are not shown. The superposition was based on the Cα carbons from residues 72–104 and 251–285.

ized inhibitor-bound complexes of CYP119 and CYP2B4 (*43*, *45*). The presence of F87 in P450BM-3 appears to greatly restrict the active site in the immediate vicinity of the heme (Figure 6). F87 is highly conserved within the CYP102 family but is very rarely a phenylalanine outside this family. The steric conflict between the imidazole ring and F87 and A264 in P450BM3 appears to reduce the ability of the imidazole to occupy the heme−iron ligand site.

The role of F87 in the structure also explains the previous observation that ω-imidazolyl fatty acid inhibitors have increased potency for the F87G mutant of P450BM-3 relative to the wild-type enzyme (*26*). The difference in free energy of binding for wild type versus F87G based on the reported $K_D$s would be 2 kJ/mol. On the basis of this information, it is possible to estimate the binding energy penalty attributed to the presence of F87. This penalty would be comprised of two components when the phenylalanine ring is present. First, some energy is required to rotate the F87 ring. Estimates for this energy from data on the binding of substrates to F87 mutants range from 0.4 to 4.6 kJ/mol, and the energy required to rotate the ring in the oxidized enzyme was estimated from computational models as 2.8 kJ/mol (*51*). The second component is the resistance of the phenylalanine residue to translation. This resistance helps to restrict the conformation of the imidazole ring to a position that requires disruption of the I-helix. The side chain of F87 prevents rotation of the imidazole ring to adopt the orientations observed in inhibitor-bound structures of P450cam (*44*), CYP119 (*45*), or CYP2B4 (*43*), where the ring is more perpendicular to the I-helix and does not perturb the I-helix significantly. The disruption of the I-helix observed upon inhibitor binding to P450BM-3 would obviously require some investment of energy. This notion is supported by the finding that the backbone ψ torsional angle for His266 is distorted to fall into the disallowed region of the Ramachandran plot (*47*). These effects underlie the low affinity for imidazole inhibitors to P450BM-3. The low change in binding energy due to the F87 side chain (2 kJ/mol) is not enough to explain the overall low affinity of imidazole compounds to the enzyme, so clearly other elements of the structure also contribute to restricting the imidazole conformation.

Perhaps the most interesting aspect of our structure is that it provides an explanation for the previous observation of cooperativity between inhibitor binding and substrate binding (*26*). Although the large fatty acid substrate arachidonic acid competed with the inhibitors as expected, the shorter fatty acid laurate actually potentiated inhibitor binding. Inhibitor

affinity increased approximately 2-fold in the presence of lauric acid. The open active site channel in the C12-Im-Leu-bound BMP structure provides a potential explanation for this observation, as the inhibitor does not seem capable of covering the hydrophobic interior surface of the channel. Addition of lauric acid would be expected to fill this void and may interact with R47 in the way observed in fatty acid bound structures of BMP, with a concomitant increase in affinity such as was observed. The unexpected open structure of the C12-Im-Leu/BMP complex provides a convenient mechanism for the observed cooperativity. A similar binding mode may be possible even in the absence of an imidazole moiety, as this enzyme has been reported to be capable of binding two different substrates simultaneously in the same active site, based on observations of substrate–substrate cooperativity, cosubstrate-dependent isotope effects, and changes in regioselectivity (*52*).

The open structure of the complex and the observed cooperativity suggest several ways to make even more potent inhibitors in the future. The fact that the acyl chain adopts multiple conformations in the open substrate access channel between the imidazole ring and the amino acid binding site suggests that addition of hydrophobic surface to the inhibitor would be beneficial. This could be accomplished by the incorporation of a longer acyl chain. The chain lengths employed in the current study were chosen on the basis of the assumption that they would follow the same pathway as fatty acid substrates. The "detour" toward V78 would require a longer acyl chain to allow the amino acid group to occupy the same site as in the acyl amino acid substrates. This assumption may in part explain why the amino acid carboxylate does not interact well with the B′-helix, because it may be restricted by the shortness of the acyl chain that is anchored to the heme iron by the imidazole ring. An alternative way to fill in the empty hydrophobic space available in the active site channel would be to add a second hydrophobic chain to the inhibitor structure to simulate the presence of both C12-Im-Leu and lauric acid in one single compound. This strategy is analogous to the design of traditional bisubstrate inhibitors. These inhibitors have a free energy of binding that is equal to the sum of the binding free energies of the two substrates (in this case inhibitor plus substrate) plus an additional increase in affinity due to a reduction in rotational and translational entropy compared to the free molecules minus a penalty for design imperfections (*53*, *54*). As a result, an acyl imidazole inhibitor covalently coupled to a lauric acid moiety in the proper orientation would bind much more tightly than even C12-Im-Leu (we estimate a $K_D$ below 0.1 nM).[2]

Adding amino acids to acyl imidazole inhibitors of P450BM-3 worked well to increase inhibitor potency as we had predicted, although the exact structural interactions responsible for the higher affinity were different than the interactions responsible for increased affinity of acyl amino acid substrates. The crystal structure of the C12-Im-Leu/BMP complex reveals these new interactions, explains the structural basis of many previously observed features of inhibitor/P450BM-3 interactions, and suggests ways to enhance inhibitor affinity in the future.

## REFERENCES


1. Palmer, C. N., Axen, E., Hughes, V., and Wolf, C. R. (1998) The repressor protein, Bm3R1, mediates an adaptive response to toxic fatty acids in *Bacillus megaterium*. *J. Biol. Chem. 273*, 18109–18116.
2. Narhi, L. O., Kim, B. H., Stevenson, P. M., and Fulco, A. J. (1983) Partial characterization of a barbiturate-induced cytochrome P-450-dependent fatty acid monooxygenase from *Bacillus megaterium*. *Biochem. Biophys. Res. Commun. 116*, 851–858.
3. Wen, L. P., and Fulco, A. J. (1987) Cloning of the gene encoding a catalytically self-sufficient cytochrome P-450 fatty acid monooxygenase induced by barbiturates in *Bacillus megaterium* and its functional expression and regulation in heterologous (*Escherichia coli*) and homologous (*Bacillus megaterium*) hosts. *J. Biol. Chem. 262*, 6676–6682.
4. Narhi, L. O., and Fulco, A. J. (1986) Characterization of a catalytically self-sufficient 119,000-dalton cytochrome P-450 monooxygenase induced by barbiturates in *Bacillus megaterium*. *J. Biol. Chem. 261*, 7160–7169.
5. Narhi, L. O., and Fulco, A. J. (1987) Identification and characterization of two functional domains in cytochrome P-450BM-3, a catalytically self-sufficient monooxygenase induced by barbiturates in *Bacillus megaterium*. *J. Biol. Chem. 262*, 6683–6690.
6. Miura, Y., and Fulco, A. J. (1975) Omega-1, Omega-2 and Omega-3 hydroxylation of long-chain fatty acids, amides and alcohols by a soluble enzyme system from *Bacillus megaterium*. *Biochim. Biophys. Acta 388*, 305–317.
7. Capdevila, J. H., Wei, S., Helvig, C., Falck, J. R., Belosludtsev, Y., Truan, G., Graham-Lorence, S. E., and Peterson, J. A. (1996) The highly stereoselective oxidation of polyunsaturated fatty acids by cytochrome P450BM-3. *J. Biol. Chem. 271*, 22663–22671.
8. Sevrioukova, I. F., Li, H., Zhang, H., Peterson, J. A., and Poulos, T. L. (1999) Structure of a cytochrome P450-redox partner electron-transfer complex. *Proc. Natl. Acad. Sci. U.S.A. 96*, 1863–1868.
9. Li, H., and Poulos, T. L. (1997) The structure of the cytochrome p450BM-3 haem domain complexed with the fatty acid substrate, palmitoleic acid. *Nat. Struct. Biol. 4*, 140–146.
10. Yeom, H., Sligar, S. G., Li, H., Poulos, T. L., and Fulco, A. J. (1995) The role of Thr268 in oxygen activation of cytochrome P450BM-3. *Biochemistry 34*, 14733–14740.
11. Haines, D. C., Tomchick, D. R., Machius, M., and Peterson, J. A. (2001) Pivotal role of water in the mechanism of P450BM-3. *Biochemistry 40*, 13456–13465.
12. Ravichandran, K. G., Boddupalli, S. S., Hasemann, C. A., Peterson, J. A., and Deisenhofer, J. (1993) Crystal structure of hemoprotein domain of P450BM-3, a prototype for microsomal P450's. *Science 261*, 731–736.
13. Yun, C. H., Kim, K. H., Kim, D. H., Jung, H. C., and Pan, J. G. (2007) The bacterial P450 BM3: a prototype for a biocatalyst with human P450 activities. *Trends Biotechnol. 25*, 289–298.
14. Pflug, S., Richter, S. M., and Urlacher, V. B. (2007) Development of a fed-batch process for the production of the cytochrome P450 monooxygenase CYP102A1 from *Bacillus megaterium* in *E. coli*. *J. Biotechnol. 129*, 481–488.
15. Appel, D., Lutz-Wahl, S., Fischer, P., Schwaneberg, U., and Schmid, R. D. (2001) A P450 BM-3 mutant hydroxylates alkanes, cycloalkanes, arenes and heteroarenes. *J. Biotechnol. 88*, 167–171.
16. Otey, C. R., Landwehr, M., Endelman, J. B., Hiraga, K., Bloom, J. D., and Arnold, F. H. (2006) Structure-guided recombination creates an artificial family of cytochromes P450. *PLoS Biol. 4*, e112.
17. Meinhold, P., Peters, M. W., Chen, M. M., Takahashi, K., and Arnold, F. H. (2005) Direct conversion of ethane to ethanol by engineered cytochrome P450 BM3. *ChemBioChem 6*, 1765–1768.
18. Munzer, D. F., Meinhold, P., Peters, M. W., Feichtenhofer, S., Griengl, H., Arnold, F. H., Glieder, A., and de Raadt, A. (2005) Stereoselective hydroxylation of an achiral cyclopentanecarboxylic acid derivative using engineered P450s BM-3. *Chem. Commun. (Cambridge),* 2597–2599.
19. Seng, W. T., Arnold, F. H., and Schwaneberg, U. (2004) Laboratory evolution of cytochrome p450 BM-3 monooxygenase for organic cosolvents. *Biotechnol. Bioeng. 85*, 351–358.
20. Peters, M. W., Meinhold, P., Glieder, A., and Arnold, F. H. (2003) Regio- and enantioselective alkane hydroxylation with engineered cytochromes P450 BM-3. *J. Am. Chem. Soc. 125*, 13442–13450.
21. Fairhead, M., Giannini, S., Gillam, E. M., and Gilardi, G. (2005) Functional characterisation of an engineered multidomain human P450 2E1 by molecular Lego. *J. Biol. Inorg. Chem. 10*, 842–853.

22. Sieber, V., Martinez, C. A., and Arnold, F. H. (2001) Libraries of hybrid proteins from distantly related sequences. *Nat. Biotechnol. 19*, 456–460.
23. Dodhia, V. R., Fantuzzi, A., and Gilardi, G. (2006) Engineering human cytochrome P450 enzymes into catalytically self-sufficient chimeras using molecular Lego. *J. Biol. Inorg. Chem. 11*, 903–916.
24. Remmer, H., Schenkman, J., Estabrook, R. W., Sasame, H., Gillette, J., Narasimhulu, S., Cooper, D. Y., and Rosenthal, O. (1966) Drug interaction with hepatic microsomal cytochrome. *Mol. Pharmacol. 2*, 187–190.
25. Peterson, J. A., Ullrich, V., and Hildebrandt, A. G. (1971) Methyrapone interaction with *Pseudomonas putida* cytochrome P-405. *Arch. Biochem. Biophys. 145*, 531–542.
26. Noble, M. A., Quaroni, L., Chumanov, G. D., Turner, K. L., Chapman, S. K., Hanzlik, R. P., and Munro, A. W. (1998) Imidazolyl carboxylic acids as mechanistic probes of flavocytochrome P-450 BM3. *Biochemistry 37*, 15799–15807.
27. Jovanovic, T., and McDermott, A. E. (2005) Observation of ligand binding to cytochrome P450 BM-3 by means of solid-state NMR spectroscopy. *J. Am. Chem. Soc. 127*, 13816–13821.
28. Ravindranathan, K. P., Gallicchio, E., McDermott, A. E., and Levy, R. M. (2007) Conformational dynamics of substrate in the active site of cytochrome P450 BM-3/NPG complex: insights from NMR order parameters. *J. Am. Chem. Soc. 129*, 474–475.
29. Hegde, A., Haines, D. C., Bondlela, M., Chen, B., Schaffer, N., Tomchick, D. R., Machius, M., Nguyen, H., Chowdhary, P. K., Stewart, L., Lopez, C., and Peterson, J. A. (2007) Interactions of substrates at the surface of p450s can greatly enhance substrate potency. *Biochemistry 46*, 14010–14017.
30. Sevrioukova, I., Truan, G., and Peterson, J. A. (1996) The flavoprotein domain of P450BM-3: expression, purification, and properties of the flavin adenine dinucleotide- and flavin mononucleotide-binding subdomains. *Biochemistry 35*, 7528–7535.
31. Boddupalli, S. S., Hasemann, C. A., Ravichandran, K. G., Lu, J. Y., Goldsmith, E. J., Deisenhofer, J., and Peterson, J. A. (1992) Crystallization and preliminary x-ray diffraction analysis of P450terp and the hemoprotein domain of P450BM-3, enzymes belonging to two distinct classes of the cytochrome P450 superfamily. *Proc. Natl. Acad. Sci. U.S.A. 89*, 5567–5571.
32. Omura, T., and Sato, R. (1964) The Carbon Monoxide-Binding Pigment of Liver Microsomes. I. Evidence for Its Hemoprotein Nature. *J. Biol. Chem. 239*, 2370–2378.
33. Lu, P., Alterman, M. A., Chaurasia, C. S., Bambal, R. B., and Hanzlik, R. P. (1997) Heme-coordinating analogs of lauric acid as inhibitors of fatty acid omega-hydroxylation. *Arch. Biochem. Biophys. 337*, 1–7.
34. Alterman, M. A., Chaurasia, C. S., Lu, P., Hardwick, J. P., and Hanzlik, R. P. (1995) Fatty acid discrimination and omega-hydroxylation by cytochrome P450 4A1 and a cytochrome P4504A1/NADPH-P450 reductase fusion protein. *Arch. Biochem. Biophys. 320*, 289–296.
35. Devadas, B., Freeman, S. K., Zupec, M. E., Lu, H. F., Nagarajan, S. R., Kishore, N. S., Lodge, J. K., Kuneman, D. W., McWherter, C. A., Vinjamoori, D. V., Getman, D. P., Gordon, J. I., and Sikorski, J. A. (1997) Design and synthesis of novel imidazole-substituted dipeptide amides as potent and selective inhibitors of *Candida albicans* myristoylCoA:protein N-myristoyltransferase and identification of related tripeptide inhibitors with mechanism-based antifungal activity. *J. Med. Chem. 40*, 2609–2625.
36. Otwinowski, Z., and Minor, W. (1997) Processing of X-ray diffraction data collected in oscillation mode. *Methods Enzymol. 276*, 307–326.
37. Jones, T. A., Zou, J. Y., and Cowan, S. W. (1991) Improved methods for building protein models in electron density maps and the location of errors in these models. *Acta Crystallogr., Sect. A: Found. Crystallogr. 47*, 110–119.
38. Brugner, A. T., Adams, P. D., Clore, G. M., DeLano, W. L., Gros, P., Grosse-Kunstleve, R. W., Jiang, J. S., Kuszewski, J., Nilges, M., Pannu, N. S., Read, R. J., Rice, L. M., Simonson, T., and Warren, G. L. (1998) Crystallography & NMR system: A new software suite for macromolecular structure determination. *Acta Crystallogr., Sect. D: Biol.Crystallogr. 54*, 905–921.
39. Murshudov, G. N., Vagin, A. A., and Dodson, E. J. (1997) Refinement of macromolecular structures by the maximum-likelihood method. *Acta Crystallogr., Sect. D: Biol. Crystallogr. 53*, 240–255.
40. DeLano, W. L. (2002) The PyMOL Molecular Graphics System, DeLano Scientific Co., Palo Alto, CA.
41. Boddupalli, S. S., Estabrook, R. W., and Peterson, J. A. (1990) Fatty acid monooxygenation by cytochrome P-450BM-3. *J. Biol. Chem. 265*, 4233–4239.
42. Zhao, Y., White, M. A., Muralidhara, B. K., Sun, L., Halpert, J. R., and Stout, C. D. (2006) Structure of microsomal cytochrome P450 2B4 complexed with the antifungal drug bifonazole: insight into P450 conformational plasticity and membrane interaction. *J. Biol. Chem. 281*, 5973–5981.
43. Scott, E. E., White, M. A., He, Y. A., Johnson, E. F., Stout, C. D., and Halpert, J. R. (2004) Structure of mammalian cytochrome P450 2B4 complexed with 4-(4-chlorophenyl)imidazole at 1.9-Å resolution: insight into the range of P450 conformations and the coordination of redox partner binding. *J. Biol. Chem. 279*, 27294–27301.
44. Verras, A., Alian, A., and de Montellano, P. R. (2006) Cytochrome P450 active site plasticity: attenuation of imidazole binding in cytochrome P450. (cam) by an L244A mutation. *Protein Eng., Des. Sel. 19*, 491–496.
45. Yano, J. K., Koo, L. S., Schuller, D. J., Li, H., Ortiz de Montellano, P. R., and Poulos, T. L. (2000) Crystal structure of a thermophilic cytochrome P450 from the archaeon *Sulfolobus solfataricus*. *J. Biol. Chem. 275*, 31086–31092.
46. Poulos, T. L., and Howard, A. J. (1987) Crystal structures of metyrapone- and phenylimidazole-inhibited complexes of cytochrome P-450cam. *Biochemistry 26*, 8165–8174.
47. Lovell, S. C., Davis, I. W., Arendall, W. B., III, de Bakker, P. I., Word, J. M., Prisant, M. G., Richardson, J. S., and Richardson, D. C. (2003) Structure validation by Calpha geometry: phi,psi and Cbeta deviation. *Proteins 50*, 437–450.
48. Murataliev, M. B., and Feyereisen, R. (1996) Functional interactions in cytochrome P450BM3. Fatty acid substrate binding alters electron-transfer properties of the flavoprotein domain. *Biochemistry 35*, 15029–15037.
49. Modi, S., Primrose, W. U., Boyle, J. M., Gibson, C. F., Lian, L. Y., and Roberts, G. C. K. (1995) NMR studies of substrate binding to cytochrome P450 BM3: comparisons to cytochrome P450 cam. *Biochemistry 34*, 8982–8988.
50. Modi, S., Sutcliffe, M. J., Primrose, W. U., Lian, L. Y., and Roberts, G. C. K. (1996) The catalytic mechanism of cytochrome P450 BM3 involves a 6 Å movement of the bound substrate on reduction. *Nat. Struct. Biol. 3*, 414–417.
51. Haines, D. C. (2006) A role for the strained phenylalanine ring rotation induced by substrate binding to cytochrome CYP102A1. *Protein Pept. Lett. 13*, 977–980.
52. Rock, D. A., Perkins, B. N., Wahlstrom, J., and Jones, J. P. (2003) A method for determining two substrates binding in the same active site of cytochrome P450BM3: an explanation of high energy omega product formation. *Arch. Biochem. Biophys. 416*, 9–16.
53. Parang, K., and Cole, P. A. (2002) Designing bisubstrate analog inhibitors for protein kinases. *Pharmacol. Ther. 93*, 145–157.
54. Page, M. I., and Jencks, W. P. (1971) Entropic contributions to rate accelerations in enzymic and intramolecular reactions and the chelate effect. *Proc. Natl. Acad. Sci. U.S.A. 68*, 1678–1683.


BI7023964